


Spatial distribution of B cells predicts prognosis in human pancreatic adenocarcinoma

Giovanni Francesco Castino, Nina Cortese, Giovanni Capretti, Simone Serio, Giuseppe Di Caro, Rossana Mineri, Elena Magrini, Fabio Grizzi, Paola Cappello, Francesco Novelli, Paola Spaggiari, Massimo Roncalli, Cristina Ridolfi, Francesca Gavazzi, Alessandro Zerbi, Paola Allavena & Federica Marchesi


To cite this article: Giovanni Francesco Castino, Nina Cortese, Giovanni Capretti, Simone Serio, Giuseppe Di Caro, Rossana Mineri, Elena Magrini, Fabio Grizzi, Paola Cappello, Francesco Novelli, Paola Spaggiari, Massimo Roncalli, Cristina Ridolfi, Francesca Gavazzi, Alessandro Zerbi, Paola Allavena & Federica Marchesi (2016) Spatial distribution of B cells predicts prognosis in human pancreatic adenocarcinoma, *Oncolmmunology*, 5:4, e1085147, DOI: [10.1080/2162402X.2015.1085147](https://doi.org/10.1080/2162402X.2015.1085147)

To link to this article: <https://doi.org/10.1080/2162402X.2015.1085147>

 View supplementary material 


 Published online: 08 Apr 2016.

 Submit your article to this journal 

 Article views: 1064

 View related articles 

 View Crossmark data 

 Citing articles: 39 View citing articles 

ORIGINAL RESEARCH

Spatial distribution of B cells predicts prognosis in human pancreatic adenocarcinoma

Giovanni Francesco Castino^a, Nina Cortese^a, Giovanni Capretti^b, Simone Serio^c, Giuseppe Di Caro^a, Rossana Mineri^d, Elena Magrini^a, Fabio Grizzi^a, Paola Cappello^e, Francesco Novelli^e, Paola Spaggiari^f, Massimo Roncalli^f, Cristina Ridolfi^b, Francesca Gavazzi^b, Alessandro Zerbi^b, Paola Allavena^a, and Federica Marchesi^{a,g}

^aDepartment of Immunology and Inflammation, Humanitas Clinical and Research Center, Rozzano, Italy; ^bSection of Pancreatic Surgery, Department of Surgery, Humanitas Clinical and Research Center, Rozzano, Italy; ^cOperational Unit of Milano; Institute of Genetics and Biomedical Research, National Research Council and Humanitas Clinical and Research Center, Rozzano, Italy; ^dMolecular Biology Section, Clinical Investigation Laboratory, Humanitas Clinical and Research Center, Rozzano, Italy; ^eCenter for Experimental Research and Medical Studies, Città della Salute e della Scienza di Torino and Department of Molecular Biotechnology and Health Sciences, University of Torino, Torino, Italy; ^fDepartment of Pathology, Humanitas Clinical and Research Center, Rozzano, Italy; ^gDepartment of Medical Biotechnologies and Translational Medicine, University of Milan, Milano, Italy.

ABSTRACT

B-cell responses are emerging as critical regulators of cancer progression. In this study, we investigated the role of B lymphocytes in the microenvironment of human pancreatic ductal adenocarcinoma (PDAC), in a retrospective consecutive series of 104 PDAC patients and in PDAC preclinical models. Immunohistochemical analysis revealed that B cells occupy two histologically distinct compartments in human PDAC, either scatteringly infiltrating (CD20-TILs), or organized in tertiary lymphoid tissue (CD20-TLT). Only when retained within TLT, high density of B cells predicted longer survival (median survival 16.9 mo CD20-TLT^{hi} vs. 10.7 mo CD20-TLT^{lo}; $p = 0.0085$). Presence of B cells within TLT associated to a germinal center (GC) immune signature, correlated with CD8-TIL infiltration, and empowered their favorable prognostic value. Immunotherapeutic vaccination of spontaneously developing PDAC (Kras^{G12D}-Pdx1-Cre) mice with α -enolase (ENO1) induced formation of TLT with active GCs and correlated with increased recruitment of T lymphocytes, suggesting induction of TLT as a strategy to favor mobilization of immune cells in PDAC. In contrast, in an implanted tumor model devoid of TLT, depletion of B cells with an anti-CD20 antibody reinstated an antitumor immune response. Our results highlight B cells as an essential element of the microenvironment of PDAC and identify their spatial organization as a key regulator of their antitumor function. A mindful evaluation of B cells in human PDAC could represent a powerful prognostic tool to identify patients with distinct clinical behaviors and responses to immunotherapeutic strategies.

Abbreviations: AICDA, activation-induced cytidine deaminase; Bcl-6, B-cell lymphoma 6; BLNK, B-cell linker; DSS, disease-specific death; ENO1, α -enolase; FFPE, formalin-fixed paraffin embedded; GC, germinal center; HEV, high endothelial venules; IFN, interferon; IRA, immune-reactive area; PD-1, programmed cell death 1; PDAC, pancreatic ductal adenocarcinoma; Tfh, T follicular helper; TGF- β , transforming growth factor- β ; TILs, tumor-infiltrating lymphocytes; TNF, tumor necrosis factor; TLT, tertiary lymphoid tissue

ARTICLE HISTORY

Received 15 July 2015
Accepted 15 August 2015

KEYWORDS

B cells; biomarkers; immunotherapy; pancreatic adenocarcinoma (PDAC); tertiary lymphoid tissue

Introduction

PDAC is the fifth leading cause of cancer-related death worldwide.¹ At diagnosis, only 20% of patients are eligible to surgery and chemotherapy has limited impact on survival,² fostering the efforts toward complementary anticancer strategies, including immunotherapy. PDAC-associated immune contexture has been investigated, both in genetic mouse models and human PDAC. It is composed by a desmoplastic stroma containing immunosuppressive cells since the very early phases of the disease^{3,4} and representing a barrier to effector T cells⁵, but also a potential target of immunotherapeutic approaches.^{4,6,7} This view has recently been challenged by studies revealing a positive effect of PDAC stromal reaction to immunotherapeutic strategies,⁸ thus reinforcing the hypothesis that a better definition of the immune environment of PDAC would help

identifying patients who are more likely to benefit from immunotherapeutic approaches.^{4,7}

In the era of personalized cancer medicine and innovative immunotherapeutic strategies, translational research has been challenged with the need of informative biomarkers to better stratify tumor patients and choose the optimal therapeutic treatment accordingly.⁹ Tumor profiles generated by standardized wide-scale analyses have highlighted a central position of immune variables in dictating tumor progression,^{9,10} suggesting that specific immune subsets should be included within the currently available TNM (Tumor-Node-Metastasis) staging system in the determination of patient's prognosis.^{11,12} Despite the advent of innovative prognostic tools, such as global molecular analyses, histopathological examination of immune cells in tumors still stands as one of the most powerful approaches to

assess the relevance of the complex immune microenvironment.

Within the tumor tissue, the organization of immune cells has emerged as an important determinant of immune cell function.¹³ According to the localization and spatial distribution of lymphocytes within tumors, various sub-components of the intratumor lymphocytic reaction can be identified, including peri- and intratumor infiltration, diffuse infiltration and, more recently defined, ectopic lymph node-like structures (or tertiary lymphoid tissue, TLT).^{12,14–18} Spatial compartmentalization of T and B lymphocytes within TLT is crucial for recruitment of tumor-infiltrating T lymphocytes (TILs),^{12,18,19} GC reactions,^{20,21} and has been shown to coordinate with TIL infiltration in predicting better clinical outcome.^{12,22} As to B cells, which represent a primary cellular constituent of TLT and an important component of the immune infiltrate in solid tumors,^{23–26} they have been largely excluded from studies addressing the clinical relevance of tumor-infiltrating cells. Yet B cells critically regulate T-cell immune responses,^{24,26–31} but their role in cancer is still controversial. B-cell activation requires proper help from follicular helper T (T_{fh}) cells, the T-cell subset residing in the B-cell area of lymphoid tissue and deputed to regulate B-cell survival and affinity maturation within GC.^{32–34} Their presence in the tumor microenvironment has been recently shown to positively impact on prognosis.³⁵

In this work, with an accurate and systematic assessment of specific immune variables, we analyzed B cells infiltrating human PDAC, in the prospect of identifying specific immune variables indicating clinically relevant immune responses. We found B cells in two histologically distinct compartments, either within tertiary lymphoid tissue (B-TLT) or interspersed at the tumor-stroma interface (B-TILs). In a mono-institutional cohort of 104 surgically resected PDAC patients, the two B-cell components identified subpopulations of PDAC patients with specific immune signatures and opposite clinical behaviors. Our results highlight the central role of B cells in the progression of human PDAC and the importance of accurately evaluating the spatial organization of the *in situ* immune reaction.

Results

Distinct spatial distribution of B cells in human PDAC

Human pancreatic adenocarcinoma is conventionally considered non-immunogenic, due to immune exclusion and a prominent infiltration of T-regulatory and immunosuppressive myeloid cells.^{3,6} Compared to normal pancreas (Fig. 1A), immunohistochemistry analysis of human PDAC specimens with an anti-CD20 antibody revealed a considerable infiltration of CD20⁺ B lymphocytes (Fig. 1B). CD20⁺ cells localized not only as irregularly interspersed cells at the tumor-stroma interface (CD20-TILs) (arrowheads in Fig. 1B and Fig. 1C), but also as dense aggregates, displaying a distinct spatial organization and located within the tumor stroma (asterisks in Fig. 1B and Fig. 1D). The absence of these configurations resembling tertiary lymphoid tissue (CD20-TLT) in the normal pancreatic tissue suggests that their neo-genesis is related to tumor occurrence. Importantly, B cells infiltrating human PDAC were preferentially located within TLT (CD20-TLT); in fact, density

of B cells in TLT, as evaluated by image analysis, was significantly higher compared to density of scattered CD20-TILs ($p < 0.0001$; Fig. 1E). A more detailed characterization of CD20-TLT aggregates revealed a spatial organization reminiscent of the lymph-node structure, with B cells (Fig. 1F) and T cells (Fig. 1G) partitioned in topologically distinct areas, containing mature dendritic cells expressing DC-LAMP (Fig. 1H). An organized network of specialized PNAd⁺ high endothelial venules (HEV) (arrowheads in Fig. 1I) and lymphatic vessels (arrowheads in Fig. 1J) confer features of TLT. The presence within lymphoid tissue of the lymph-organogenic chemokines CXCL13 (Fig. 1K) and CCL21 (Fig. 1L), involved in recruitment of B and T lymphocytes and in their mutual segregation, suggests an immunological task for TLT in the microenvironment of human PDAC.

Dichotomy of B cell prognostic impact in human PDAC

We sought to determine whether the dual pattern of B-cell infiltration within pancreatic tissue reflects a distinct prognostic value. Therefore, we addressed the clinical significance of B cells in human PDAC considering CD20-TLT and CD20-TILs as distinct populations. In a retrospective study, we quantitatively evaluated the percentage of immune-reactive area (IRA%) of the CD20-TLT and CD20-TILs at the tumor-stroma interface, in 104 tissue specimens from consecutive, non-metastatic PDAC patients. Distributions of immune populations according to the patient histopathological features are described in Table S1. Considering the overall population, CD20-TLT immuno-reactive area (IRA%) ranged from 0% to 23.49%, with a median value of 3.72% (second–third quartiles, 1.71%–5.71%), while CD20-TIL IRA% ranged from <0.05% to 1.89%, median value 0.41% (second–third quartile 0.26%–0.69%) (Table S1). We recorded 38 events of disease-specific death (DSS) in 104 PDAC patients, during the follow-up period of the study. Cox multivariate analysis showed that nodal status and grade associated to prognosis; notably, among the immune variables analyzed, B cells were independently associated to prognosis, but their prognostic value diverged according to their spatial distribution in the tissue. CD20-TLT associated with better prognosis (OR = 0.24; 95% CI (0.08–0.71); $p = 0.010$, 4th vs. 1st quartile; Table 1), while CD20-TILs associated to worse prognosis (OR = 2.56; 95% CI (0.91–7.23); $p = 0.07$, 3rd versus 1st quartile; Table 1). This result highlights B cells as prognostic variables in human PDAC and suggests that the influence of B cells on tumor progression changes whether they are confined within lymphoid tissue or are scattered at the tumor-stroma interface. Accordingly, Kaplan–Meier survival analysis showed that only high density of CD20-TLT (2nd–4th vs. 1st) correlated to better prognosis (median survival 16.9 mo CD20-TLT^{hi} versus 10.7 mo CD20-TLT^{lo}; $p = 0.0085$; $n = 104$; Fig. 2A), while high CD20-TIL density (3rd–4th vs. 1st–2nd) had a propensity to associate to worse prognosis but not significantly (median survival 12.7 mo CD20-TILs^{hi} versus 18.9 mo CD20-TILs^{lo}; $p = 0.115$; $n = 104$; Fig. 2B). When we considered the two variables concomitantly, the immune signature comprising CD20-TLT^{hi}

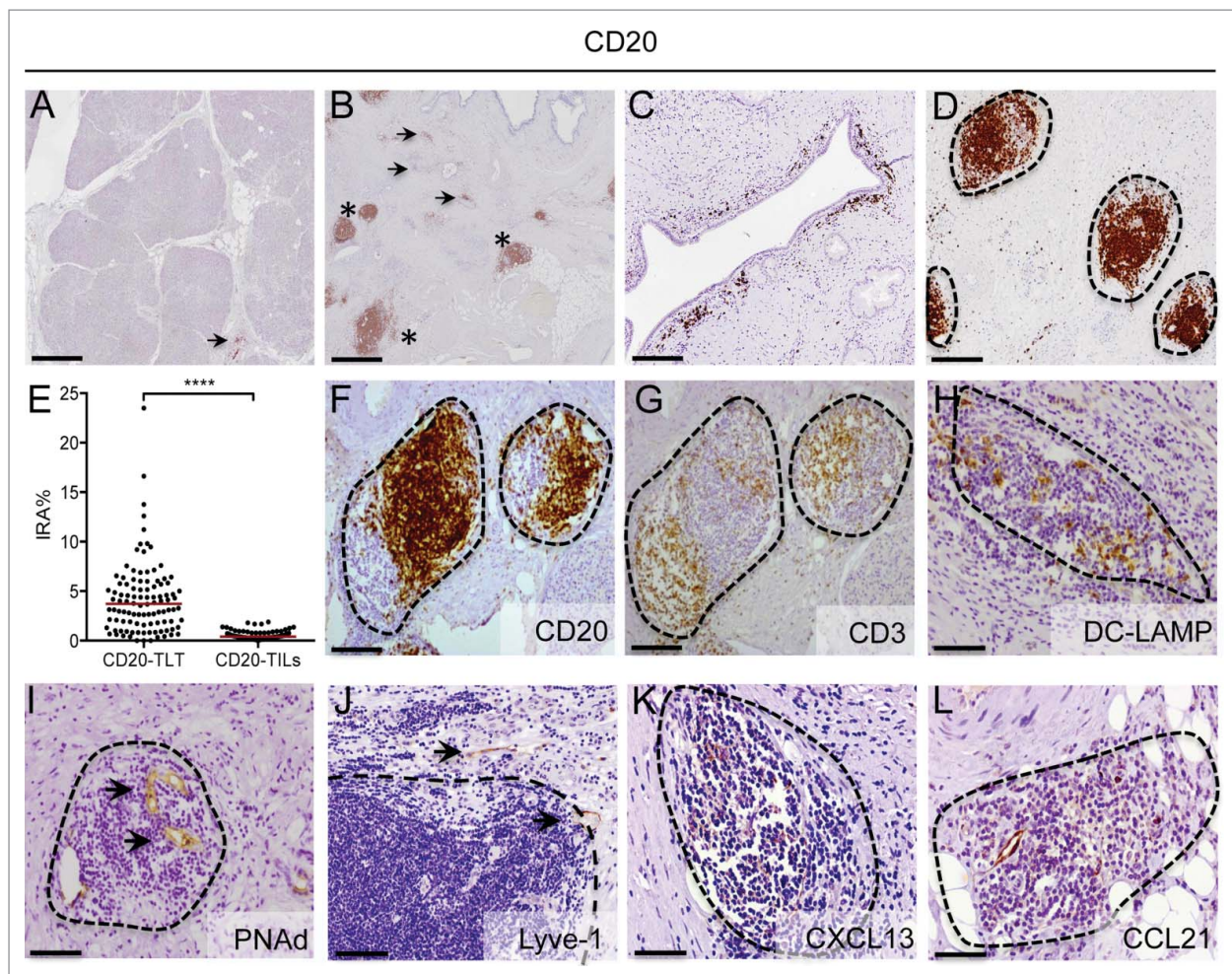


Figure 1. B cells strategically localize in tertiary lymphoid tissue in human pancreatic adenocarcinoma. (A–D) Representative images obtained from virtual digital slides of human normal pancreas (A) and pancreatic cancer (B–D), stained for CD20⁺ B cells. Staining with an anti-CD20 antibody shows few B cells distributed in normal pancreas (arrowhead in A) and at the tumor stroma-interface in PDAC (arrowheads in B and C), while the majority of B cells is located within dense aggregates (asterisks in B and D). (E) Quantitative evaluation of the density of B cells according to their localization within CD20-TLT or as CD20-TILs in tissue specimens from 104 PDAC patients. Density of B cells in TLT (CD20-TLT IRA%) was significantly higher compared to density of scattered CD20-TILs (CD20-TILs IRA%) (****: $p < 0.0001$ by Student's t test). (F–L) Lymphoid aggregates (dotted lines) in human PDAC specimens are composed of CD20⁺ B cells (F), CD3⁺ T cells (G) and mature dendritic cells expressing DC-LAMP (H). Sections in (F) and (G) panels are consecutive and show the topological compartmentalization of B and T cells. An organized network of specialized PNAAd⁺ high endothelial venules (HEV) (I) and Lyve-1⁺ lymphatics (J) confirms that the aggregates have features of tertiary lymphoid tissue (TLT). The lymphoid chemokines CXCL13 (K) and CCL21 (L) are present inside lymphoid aggregates. Dotted lines indicate follicle contour. Bars: (A–B) 500 μ m, (C–H) 200 μ m, (I–L) 100 μ m.

/CD20-TIL^{lo} robustly predicted longer survival (median survival 30.9 mo CD20-TLT^{hi}/CD20-TILs^{lo} vs. 14.1 mo any other; $p = 0.0051$; $n = 104$; Fig. 2C), confirming that the histological configuration of B cells dictates their prognostic behavior, with only B cells sequestered within a lymphoid tissue contrasting tumor progression.

Confinement of B cells within TLT associates to a germinal center immune signature, correlates with CD8-TIL infiltration, and empowers their favorable prognostic value

To understand how B cells differently regulate the local immune network according to their spatial organization, we analyzed the immune signature of PDAC tumors with very high density of TLT (4th quartile; TLT^{hi}) compared to tumors with very high density of TILs (4th quartile; TILs^{hi}), by mRNA expression analysis. Non-tumor pancreatic tissue was taken as

control tissue. Hierarchical clustering analysis revealed TLT^{hi} versus TILs^{hi} samples segregating together, suggesting that classification of tumor specimens according to the distribution of B cells identifies specific gene expression programs (Fig. S1). PDAC specimens with high density of TLT showed major changes in genes related to GC reaction (activation-induced cytidine deaminase (*AICDA*), B-cell recent activation (*CD27*), B-cell signaling ((B-cell linker (*BLNK*), B-cell differentiation and proliferation (interleukin-7 (*IL7*) and interleukin-2 (*IL2*)) and B-cell responses (interleukin-13 (*IL13*)) (Fig. 3A). Notably, while TLT^{hi} PDAC samples exhibited a significant increase in genes related to T-cell infiltration (*CD8B*) and activation (*IL-12*) (Fig. 3A), suggesting that the presence of B cells within TLT was also regulating T-cell recruitment and activation, TILs^{hi} samples exhibited increased expression in immunosuppressive genes, including programmed cell death-1 ligand (*PDL-1* or *CD274*), *CCR4* and transforming-growth factor- β (*TGF- β*). Immunohistochemical analysis confirmed that B cells within

Table 1. Predictors of post-surgical disease-specific survival in 104 patients with pancreatic ductal adenocarcinoma.

		Univariate analysis ^a		Multivariate analysis ^a Analysis ^a	
		O.R. (95%CI.)	<i>p</i>	O.R. (95%CI.)	<i>p</i>
Patient Demographics					
Age ^c		1.04 (1.00–1.07)	0.022	1.04 (1.00–1.07)	0.051
Gender	Female	1.00 ref.			
	Male	1.09 (0.58–2.07)	0.782		
Tumor Features					
Nodal involvement	No	1.00 ref.		1.00 ref.	
	Yes	2.13 (1.03–4.41)	0.020	2.55 (1.10–5.90)	0.029
	na				
Grade ^d	G1/G2	1.00 ref.		1.00 ref.	
	G3/G4	2.74 (1.37–5.49)	0.004	2.42 (1.16–5.04)	0.018
	na				
Radical ^e surgery	R0	1.96 (0.93–4.14)	0.078		
	R1	1.00 ref.			
	na				
Chemotherapy (CTX)					
Adjuvant treatment	No	1.00 ref.			
	Yes	1.03 (0.52–2.04)	0.942		
Tumor Immune features					
CD20-TLT (quartiles) ^b	1st (0–1.71)	1.00 ref.		1.00 ref.	
	2nd (1.71–3.72)	0.40 (0.16–0.98)	0.045	0.41 (0.14–1.16)	0.093
	3rd (3.72–5.71)	0.38 (0.16–0.94)	0.035	0.31 (0.09–1.04)	0.057
	4th (5.71–23.49)	0.40 (0.16–0.98)	0.044	0.24 (0.08–0.71)	0.010
CD20-TILs (quartiles) ^b	1st (0–0.26)	1.00 ref.		1.00 ref.	
	2nd (0.26–0.41)	1.30 (0.50–3.36)	0.594	1.14 (0.39–3.40)	0.807
	3rd (0.41–0.69)	2.88 (1.18–7.03)	0.020	2.56 (0.91–7.23)	0.075
	4th (0.69–1.89)	1.23 (0.46–3.30)	0.674	1.35 (0.40–4.49)	0.626
CD8-TILs (quartiles) ^b	1st (0.0–0.34)	1.00 ref.			
	2nd (0.34–0.61)	0.51 (0.22–1.23)	0.135		
	3rd (0.61–1.15)	0.89 (0.39–2.07)	0.797		
	4th (1.15–3.42)	0.69 (0.27–1.77)	0.445		
PD-1 GC	Yes	1.00 ref.			
	No	1.47 (0.72–2.99)	0.285		

^aCOX regression analysis.^bDensities as percent immune-reactive area at the tumor-stroma interface.^cAge was entered as continuous variable.^dG1/G2, well- to moderately differentiated; G3, G4 poorly differentiated.^eR0, microscopic radical resection; R1, microscopic non-radical resection.

TLT were often engaged in a GC reaction, as evidenced by Ki67 immunostaining (arrowheads in Fig. 3B, upper panel) and B-cell lymphoma 6 protein (Bcl-6) (arrowhead in Fig. 3B, lower panel).

CD8⁺ T cells are essential constituent of the antitumor immune response. In light of the association between TLT and CD8 in gene expression analysis, we assessed the density of tumor-infiltrating CD8⁺ T-cells (CD8-TILs) in the 104 PDAC patients (Fig. S2). CD8-TIL IRA% ranged from <0.1% to 3.42%, with a median value of 0.61% (second–third quartiles, 0.34%–1.12%) (Table S1). Notably, whole tissue visualization of CD8⁺-infiltrating cells evidenced a higher density of CD8-TILs in tissues with a high density of TLT (arrowheads in Fig. 3C). In fact, density of CD20-TLT correlated with the IRA% of CD8-TILs ($r = 0.29$, $p = 0.009$, $n = 104$) (Fig. 3D), consistent with the ability of TLT to mediate recruitment of lymphocytes.¹² While CD8-TILs were not associated to prognosis on their own (median survival 15.5 mo CD8-TILs^{hi} vs. 14.2 mo CD8-TILs^{lo}; $p = 0.254$, $n = 104$) (Table 1 and Fig. 3E), concomitant high density of CD8-TILs (2nd–4th quartiles) and high density of CD20-TLT (2nd–4th quartiles) identified a

subgroup of patients with better outcome compared to other patients (median survival 17.9 mo CD20-TLT^{hi}/CD8-TILs^{hi} versus 12.2 mo CD20-TLT^{lo}/CD8-TILs^{hi}; $p = 0.026$, $n = 65$) (Fig. 3F), suggesting that the presence of TLT empowers the prognostic function of CD8⁺ T cells.

PD-1⁺ follicular helper T cells within TLT germinal centers regulate B-cell localization in PDAC tissue

We then moved on to determine specific elements inside TLT, which could be associated to the dual function of B cells. Within the B-cell area of TLT (Fig. 4A), it was often possible to distinguish a peculiar cellular entity resembling a GC, characterized by the presence of PD-1⁺ cells (Fig. 4B). This suggests that they could be T-helper follicular cells (Fig. 4C), an important sub-population of T cells with a key role in the GC reaction and B-cell activation.^{32,33} To investigate whether the presence of this cell subset within the GC of TLT could have an impact on B-cell prognostic function, we quantified the GCs expressing PD-1 (PD1-GC) in all the 104 PDAC patients. PD-1-GC cells were present in 32 out of 104 (30.8%) patients. Notably,

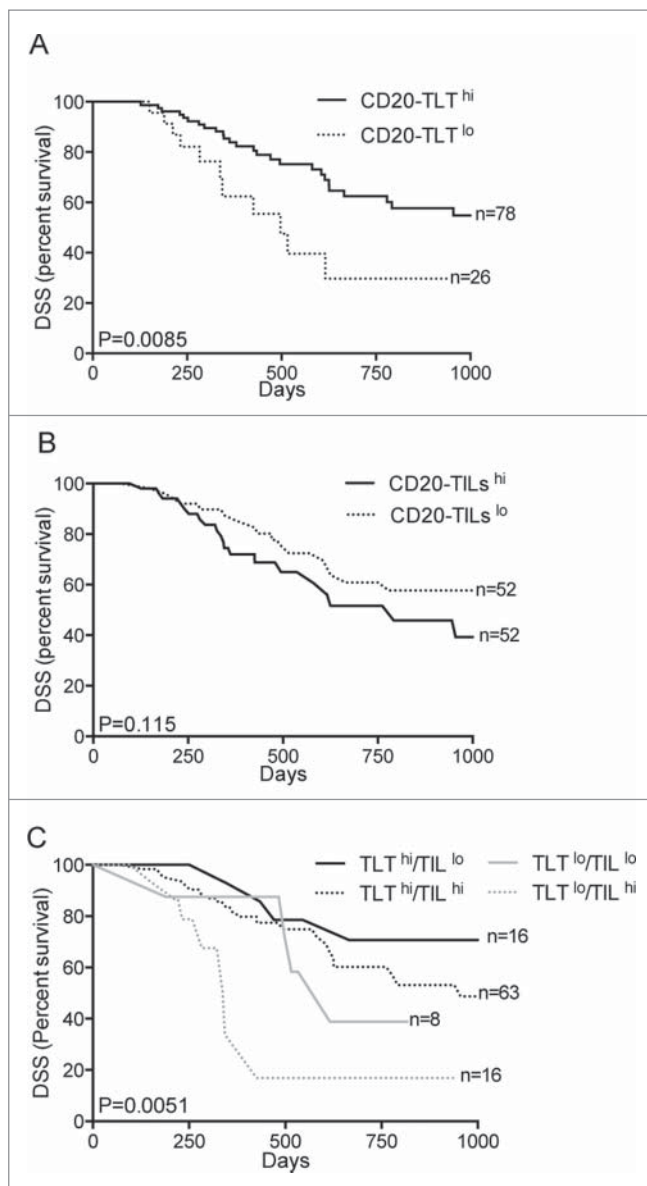


Figure 2. B cell spatial organization impacts in human PDAC prognosis. (A–C) Distinct spatial localization of B cells in the tumor microenvironment dictates their prognostic behavior. Kaplan–Meier survival analyses show correlation of high density of CD20-TLT (2nd–4th quartiles) with longer disease specific survival ($p = 0.0085$; $n = 104$) (A), while high density of CD20-TILs (3rd–4th quartiles) shows a tendency to associate to worse prognosis ($p = 0.115$; $n = 104$) (B). The immune signature comprising CD20⁺ TLT^{hi}/CD20⁺ TIL^{lo} robustly predicts longer survival ($p = 0.0051$; $n = 104$) (C). p value by Wilcoxon–Mantle Cox test.

comparing PDAC tissues with and without PD1-GC cells, the number of patients with high density of TLT was significantly higher in the PD1-GC group compared to tissues with low density of TLT ($n = 26$ vs. $n = 6$, $p < 0.0001$), suggesting that the presence of this subset is key to the formation of TLT within the tumor microenvironment (Fig. 4D). Surprisingly, in patients with PD1-GC there was no correlation of CD20-TLT with CD20-TILs ($r = -0.001$, $p = 0.559$, $n = 32$) (Fig. 4E), while the two B-cell components correlated in specimens without PD1-GC ($r = 0.39$, $p = 0.001$, $n = 70$) (Fig. 4F), suggesting that the presence of PD1-GC cells could be an important factor favoring B-cell retention within TLT and preventing B-cell scatter distribution within the tissue.

Antigen-specific immunotherapeutic vaccination induces neogenesis of intratumor TLT with PD-1⁺ germinal centers in a preclinical model of PDAC

The presence of immunologically active TLT could be of remarkable importance in the perspective of inducing a local antitumor immune response. Several immunotherapeutic approaches are under evaluation in human PDAC, including vaccination protocols directed against PDAC antigens, which would benefit from a microenvironment favorable for TLT induction. We therefore investigated whether a DNA vaccination could induce formation of TLT in a genetic preclinical model of PDAC. Vaccination of tumor-bearing mice with a vector encoding the glycolytic enzyme ENO1 has been shown to have a protective effect in Kras^{G12D}-Pdx1-Cre mice.³⁶ Hematoxylin–eosin analysis of PDAC confirmed the sporadic occurrence of TLT in PDAC tumors (Fig. S3). However, mice injected with ENO1-vaccine had a significant increase of number and surface of TLT, compared to both untreated and mice injected with empty vector (Fig. 5A–B), suggesting that vaccination induces recruitment and spatial organization of lymphocytes in the microenvironment. Remarkably, analysis of PD1-GC highlighted a robust increase in ENO1-vaccinated mice compared to controls (Fig. 5C–D), demonstrating that vaccination is able to break the immunosuppressive barrier, inducing a specific *in situ* immune reaction. The increase was paralleled by an increase in CD3-TILs, suggesting that induction of TLT by immunotherapeutic approaches could be strategic to increase recruitment of T cells (Fig. 5E–F). Importantly, vaccination resulted in long-lived systemic protective immunity, as evidenced by a rise of ENO1-specific T cells able to secrete IFN γ in ENO1-vaccinated mice compared to mice vaccinated with the empty vector (Fig. 5G).

Targeting tumor-infiltrating B cells unleashes the antitumor immune response in murine PDAC

B cells are considered practicable therapeutic targets to inhibit unwanted immune responses in the pathogenesis of immune diseases, including cancer.³⁷ However, our data showing the dual role of B cells in human PDAC question this concept in the context of solid tumors. To clarify this point, we tested the effect of a (mouse) anti-mouse CD20 antibody targeting B cells (clone 5D2, Genentech) in an implantable model of PDAC, by injecting the antibody 3 days post tumor injection. Differently from the genetic model previously mentioned, we did not observe formation of B-TLT in any of the orthotopically implanted mice (Fig. S3), likely due to the rapid tumor growth (21 d) and absence of chronic inflammatory reaction. In contrast, scattered B cells (B-TILs) infiltrated the tumor tissue (Fig. S3), confirming that B-TILs act independently from B-TLT. Circulating B cells were dramatically depleted by a single injection of the antibody (Fig. 6A), and the effect persisted until the end of the experiment (Fig. 6B), while the number of other circulating leukocytes (including CD3⁺ T cells and CD11b⁺ myeloid cells) was not significantly affected (Fig. S4). Consistent with the reduction of circulating B cells, the number of B220-TILs scattered in the tumor microenvironment was significantly reduced by the treatment (Fig. 6C–E), suggesting that

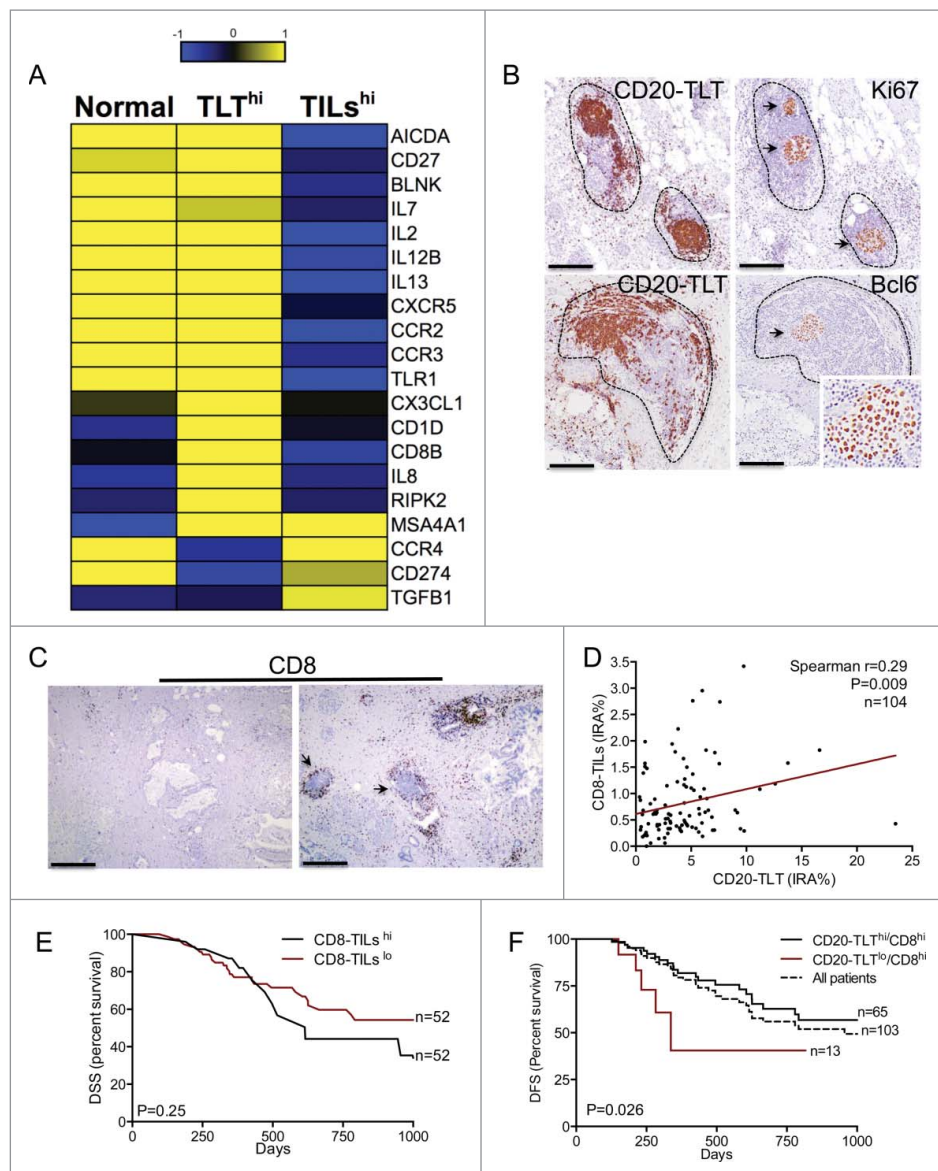


Figure 3. Confinement of B cells within TLT associates to a specific immune signature, correlates with CD8-TIL infiltration, and empowers the favorable prognostic value of CD8-TILs. (A) Heatmap showing the immune signature of human PDAC specimens with different CD20 distributions. RNA was extracted from paraffin embedded tissue specimens of human PDAC, categorized as TLT^{hi} (n = 3) or $TILs^{hi}$ (n = 3) after immunohistochemical evaluation with an anti-CD20 antibody. RNA from normal pancreata (n = 3) was obtained as a control. Sample grouping followed the pattern of B-cell distribution (i.e. TLT^{hi} vs. $TILs^{hi}$ samples segregating together), suggesting that B-cell infiltration identifies specific gene expression programs. (B) Presence of germinal center in CD20-TLT. B cells within TLT are engaged in a germinal center reaction, as evidenced by Bcl6 (arrowheads in lower right panel) and Ki-67 (arrowhead in upper right panel) staining within CD20-TLT (left panel). Left and right sections are consecutive sections. (C–F) CD20-TLT correlates with density of CD8⁺ T cells in human PDAC and empowers their prognostic function. Representative images obtained from virtual digital slides of human PDAC specimens stained with an anti-CD8 antibody show a high density of CD8⁺ cells in tissues with TLT (C). Density of CD20-TLT (IRA%) linearly correlates with density of CD8-TILs (IRA%) ($r = 0.29$, $p = 0.009$, $n = 104$) (D). (E) Kaplan–Meier curve showing that while high density of CD8-TILs (2nd–4th quartiles) is not significantly associated to prognosis ($p = 0.254$, $n = 104$), concomitant high density of CD8-TILs (2nd–4th quartiles) and high density of CD20-TLT (2nd–4th quartiles) identifies a subgroup of patients with longer disease-specific survival ($p = 0.026$; $n = 65$) (F). p value by Pearson's simple linear regression analysis in (D) and by Wilcoxon–Mantle Cox test in (E–F). Bars: 200 μ m (B); 500 μ m (C).

B220-TILs are recruited from a circulating pool of B cells. Notably, single injection of anti-CD20 slightly reduced the tumor size, albeit not significantly, suggesting a pro-tumor function of B-TILs in PDAC (Fig. 6F).

To analyze the impact of B-TIL depletion, we compared the immune signature of the leukocyte population isolated from PDAC tumors from control and α -CD20 treated mice. Depletion of tumor-infiltrating B cells resulted in a significant increase in genes related to T cell and NK cell infiltration (*CD4*, *CD8*, *NCR1*), activation (*GMZA*, *GMZB*, *IL12*, *IFNG*, and

TNFA) and recruitment (*CXCR3*) (Fig. 6G). These results show that, in an implanted tumor model devoid of B220-TLT, depletion of tumor-infiltrating B cells (B-TILs) increases the recruitment of important components of the antitumor immune response. This was not ascribable to a compensatory increase of circulating T cells, which were not significantly affected by the α -CD20 treatment (Fig. S4).

To gain more insights on the biological relevance of the signature obtained, we interrogated the set of genes by a systems biology approach based on Ingenuity Pathway Analysis

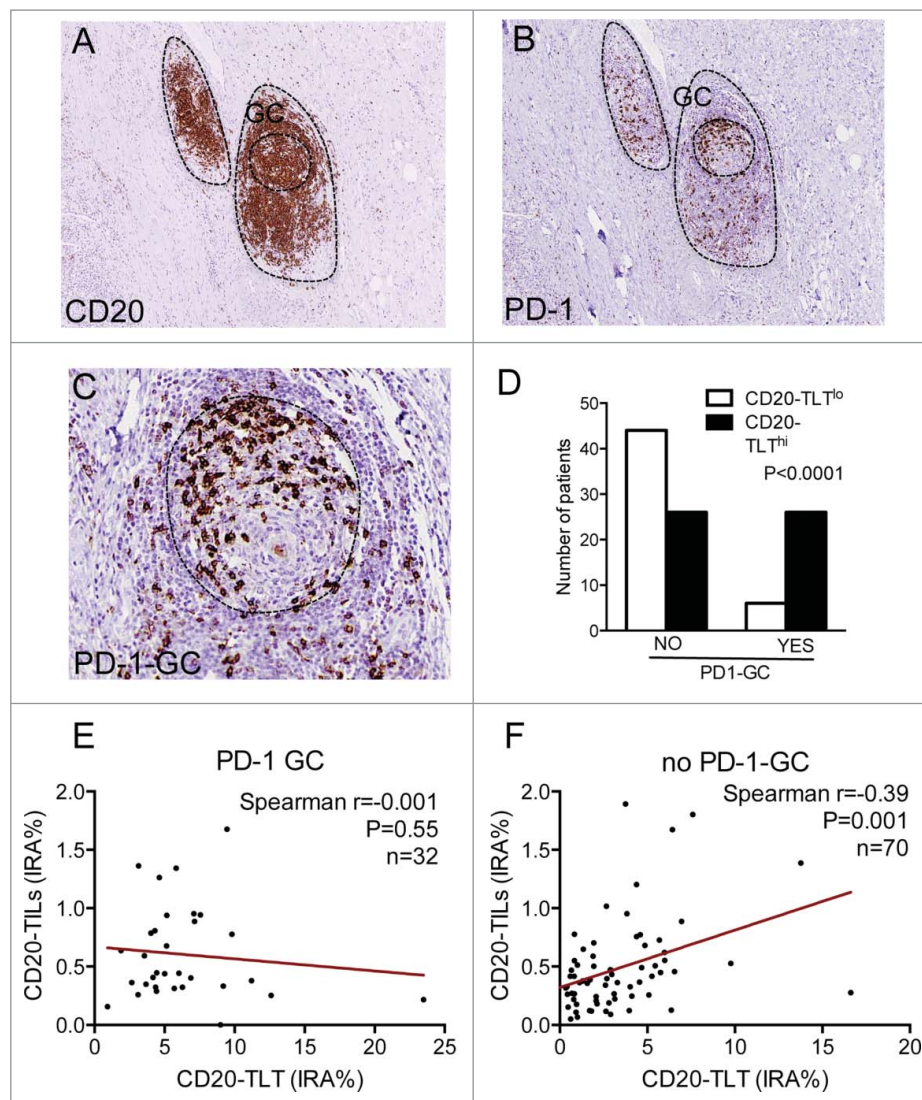


Figure 4. PD-1⁺ follicular helper T cells within TLT germinal centers regulate B-cell localization in human PDAC. (A–C) Presence of PD-1⁺ cells within germinal centers of CD20-TLT in human PDAC. Within the B-cell zone of TLT (A), there are PD-1⁺ cells (B), some of which distributed in the germinal center, suggesting they could be T-helper follicular cells (C). (D) The number of patients with high density of TLT is significantly higher in the PD1-GC group compared to specimens with low density of TLT ($p < 0.0001$). (E–F) Lack of correlation of CD20-TLT and CD20-TILs in patients with PD-1-GC ($r = -0.001$, $p = 0.559$, $n = 32$) (E), while the two B-cell components correlate in specimens without PD1-GC ($r = 0.39$, $p = 0.001$, $n = 70$) (F), suggesting that the presence of PD1-GC could be an important factor favoring B-cell aggregation in TLT and preventing B-cell scattering within the tissue. p value by Chi-square in (D), Pearson's simple linear regression analysis in (E–F). Bars: 200 μ m (A–B); 50 μ m (C).

(IPA, <http://www.ingenuity.com>). Surprisingly, within the panel of genes analyzed (Fig. S5), depletion of B cells with α -CD20 induced significant functional enrichment of genes involved in lymphoid tissue structure and development, CD8⁺ T cell infiltration and maintenance and differentiation of T cells (Fig. 6H), confirming that B-TILs are detrimental to an effective antitumor immune response.

Discussion

The ability of the immune system to contrast tumor growth hinges on the induction of an antigen-specific T-cell response.³⁸ Surprisingly, despite anticancer effects are rarely ascribed to B-cell-mediated functions, increasing evidence that B cells play a role in cancer progression has been provided,^{23–26,29–31} bringing up the hypothesis that also B-cell responses should be considered as targets of immunotherapeutic approaches. Data herein presented suggest a dual prognostic behavior of B cells in

human cancer, which is tightly linked to their topological organization within the microenvironment. Rather than scattered in the tumor tissue, the majority of B cells was strategically located in association with T cells, within highly organized lymphoid tissue, possibly reflecting how B and T cells interact during the organization of a local immune response. Only when confined within a lymphoid site, B cells predicted better prognosis and associated to a follicular signature, suggesting that they could be involved in an ongoing follicular immune response with a protective antitumor role. Moreover, in human PDAC, CD20-TLT correlated with CD8⁺ T-cell infiltration, suggesting that B cells within TLT could concomitantly be engaged in humoral and T cell responses. In this regard, tumor-antigen-specific immunoglobulins can be crucial triggers of anticancer cellular immune responses.³¹

In contrast to B cells organized in TLT, scattered distribution of B cells in the tumor tissue was not essential to their antitumor function, in sharp opposition to what observed for T

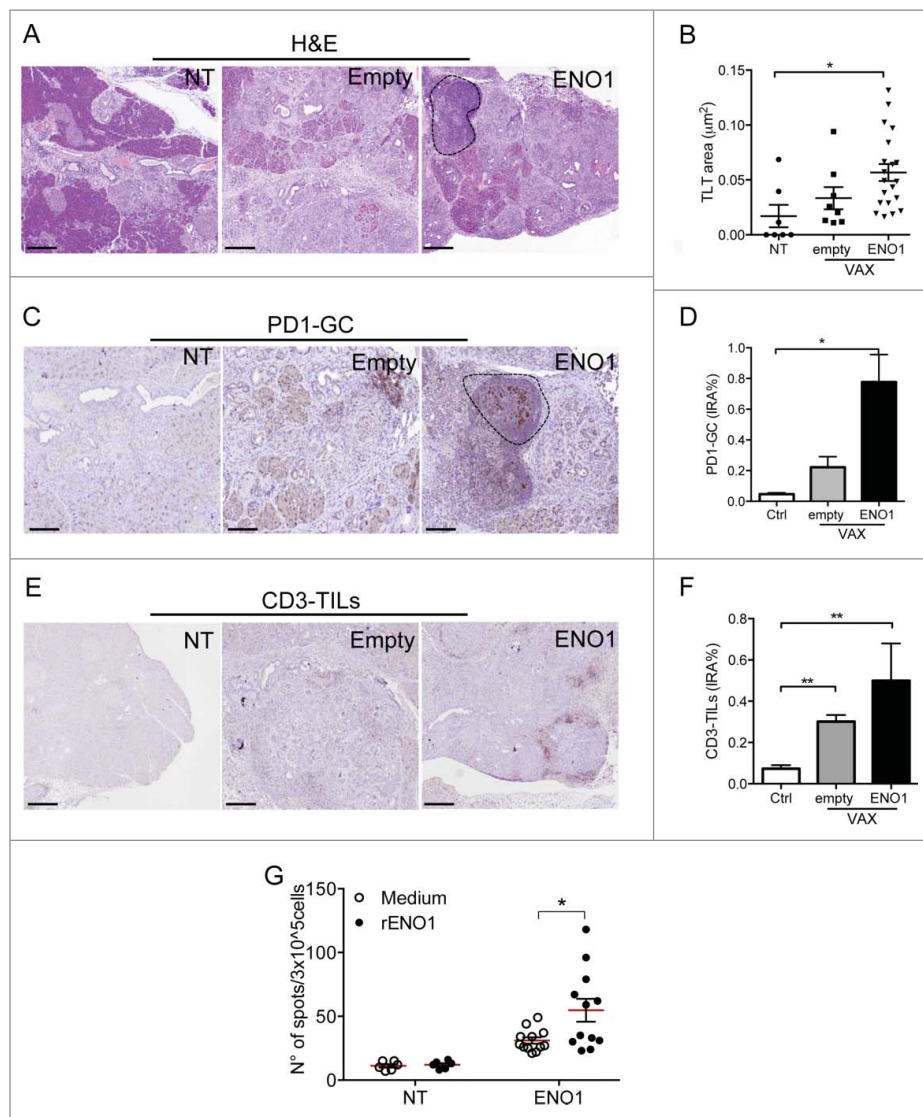


Figure 5. An immunotherapeutic DNA-vaccine induces neogenesis of intratumor TLT with active germinal centers in a preclinical model of PDAC. (A–F) Induction of TLT by an antitumor vaccination in *Kras*^{G12D}-*Pdx1*-Cre mice. Histological sections of murine PDAC from non-treated mice (NT) or mice vaccinated with empty vector (empty) or a vector encoding ENO1 (ENO1) stained with hematoxylin–eosin (A), PD-1 (C), CD3 (E). Dotted line indicates an intratumor TLT (A) or PD1-GC (C). Number and area of TLT (B), IRA% of PD1-GC (D) and CD3-TILs (F) are significantly increased by vaccination compared to untreated mice. (G) ENO1 vaccination induces specific T-cell response. Spleen cells from untreated or ENO1-vaccinated mice were stimulated on an enzyme-linked immunosorbent spot plate in the presence (black dots) or not (with dots) of rENO1. Anti-ENO1 T cells are significantly induced in ENO1-vaccinated mice, but not in untreated mice. Numbers in the graph represent the mean number of specific spots subtracted from that of background. All conditions were in triplicate. *p* value by Student's *t* test. *: *p* < 0.05; **: *p* < 0.01. Scale bar 500 μm .

cells, whose localization within the tumor is critical to predict better prognosis.¹² On the basis of our clinical and preclinical data, we hypothesize that the egress of B cells into the tissue is detrimental to an effective antitumor response and might reflect a non-specific pro-tumor inflammatory reaction. In accordance, depletion of tumor-infiltrating B cells was effective in reinstating a CD8⁺ antitumor immune response in a PDAC preclinical model without TLT. The role of B cells in the progression of solid tumors has fostered studies concerning their targeting by anti-CD20 antibodies.^{26,37,39,40} Based on our data, the design of anticancer strategies envisaging the depletion of B cells should take into account the possibility to selectively target CD20-TILs but not CD20-TLT. Interestingly, the kinetic of B cell depletion by anti-CD20 antibodies varies among different B-cell sub-populations (i.e. circulating, marginal zone, peritoneal).⁴¹ Moreover, in non-tumor conditions, anti-CD20

therapy has resulted ineffective in depleting CD20⁺ cells in tertiary lymphoid organs,⁴² suggesting that B cells might receive survival signals within lymphoid niches.⁴¹ The differential sensitivity that B cells display to anti-CD20 treatment according to their localization could be exploited to design-tailored approaches, assuming that a rigorous evaluation of B-cell spatial distribution is performed.

Whether B cells regulate protective T-cell immunity or produce tumor-specific antibodies, both actions are highly favored by the interaction with T cells within the GC. In our analysis, we identified PD1 expressing Tfh cells as a critical subset of T cells possibly involved in the successful retention of B cells within TLT. Tfh cells take part in various steps leading to GC reaction and differentiation of memory B cells and plasma-cells.³⁴ The PD-1/PD-1L network is emerging as a major inhibitory pathway associated with T-cell exhaustion in the tumor

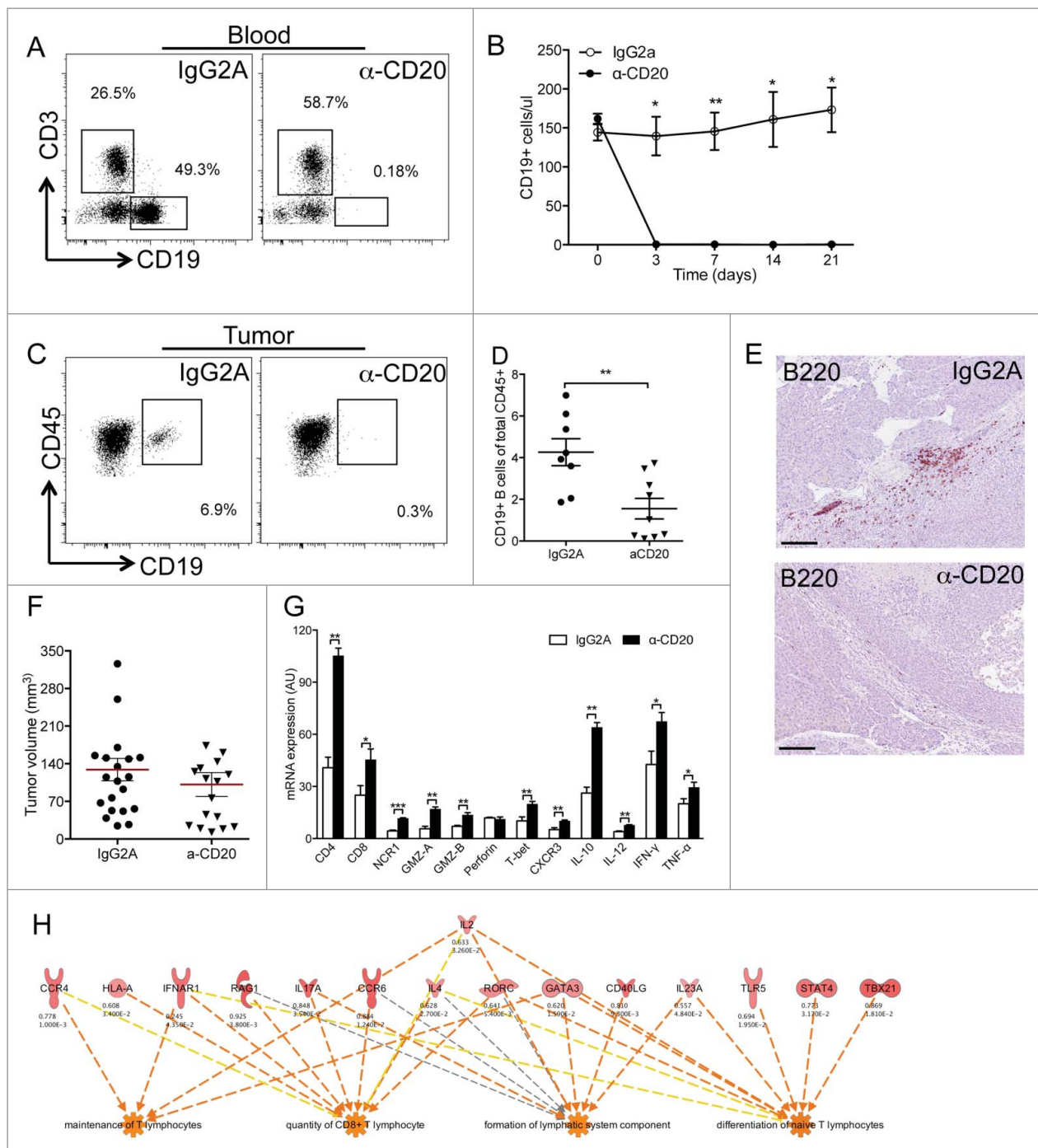


Figure 6. Targeting tumor-infiltrating B cells unleashes immune response in murine PDAC. (A–F) Depletion of B cells by an anti-CD20 antibody in a murine implantable PDAC model. Mice were orthotopically injected with the PDAC cell line Panc02 and administered either irrelevant antibody (IgG2A) or α-CD20 on day 3 post injection. (A) Exemplificative facs plot showing depletion of circulating blood CD19⁺ B cells. (B) B-cell depletion started at day 3 and lasted until the end of the experiment. One independent experiment repeated three times is shown (n = 3 mice, IgG2A; n = 4 mice α-CD20; bars represent SEM; *p < 0.05; **p < 0.01). (C) Exemplificative facs plot showing depletion of tumor infiltrating CD19⁺ B cells. (D) Percentage of CD19⁺ B cells infiltrating PDAC tumors is reduced by α-CD20 treatment. One exemplificative of three experiments performed is shown (n = 8 mice, IgG2A; n = 9 mice α-CD20; bars represent SEM; p = 0.004 by Students' t test). (E) Immunohistochemical evaluation of B cells in PDAC. Representative pictures showing reduction of B-TILs in the pancreas of α-CD20 treated mice. (F) Tumor growth was slightly but not significantly reduced by α-CD20 treatment. Mean of three independent experiments is shown (n = 20 mice, IgG2A; n = 16 mice α-CD20; bars represent SEM; p = ns by Students' t test). (G–H) Immune signature after α-CD20 treatment. RNA from leukocytes isolated from PDAC of mice treated with IgG2A or α-CD20 shows induction of genes related to T-cell infiltration and activation (G). Systems biology analysis showing the relationship between molecules and biological functions based on the genes modulated after depletion of B cells. The analysis highlights significant activation of biological functions related to lymphoid tissue structure and development, CD8⁺ T cell infiltration and maintenance and differentiation of T cells (H).

microenvironment^{43,44} and more recently also identifying immunosuppressive B cells.³⁰ Our findings, showing that PD-1 expression could identify fully competent lymphoid tissue, are counterintuitive considering the ongoing efforts aimed at

targeting this inhibitory pathway in human cancers. However, while PD-1 expression in peripheral tissues associates to immunosuppressive function, PD-1 upregulation in lymphoid tissues is an early event of T-cell activation and identifies clonally

expanded tumor-reactive T cells.⁴⁵ Therefore, PD-1 expression in GCs within TLT could indicate a T-cell recent activation, irrespective of its immunosuppressive role when engaged by the ligand. This eventually suggests that immunotherapeutic strategies targeting PD-1 could concomitantly act on exhausted T cells as well as enhance recently activated T cells. As for B cells, our data suggest that a careful evaluation of immune cells within the microenvironment is required in order to allocate the best therapeutic treatment.

The immunosuppressive nature of the tumor microenvironment and the defective localization of adoptively transferred immune cells at the tumor site blunt the efficacy of immunotherapy, favoring T-cell exclusion and immune ignorance.⁴⁶ The presence of an ectopic lymphoid site as TLT could overcome these obstacles, by providing a local immune site sustaining lymphocyte traffic, favoring *in situ* T-cell activation and immunoglobulin secretion.⁴⁷ In this regard, allogeneic immunoglobulins, as the ones elicited during vaccination could enhance the efficacy of combined immunotherapeutic approaches and favor T-cell antitumor immune response.³¹ Importantly, the association of TLT with better prognosis in human PDAC patients suggests that the immune response induced could be protective overtime; this was confirmed in our genetic preclinical model, where vaccination induced expansion of antigen-specific IFN γ -secreting cells and cytotoxic serum antibodies.³⁶ Our findings, while supporting the hypothesis that effective immunotherapeutic strategies should be licensing the tumor contexture to immune infiltration, highlights TLT as instrumental to clinical benefit. In our cohort, TLT occurrence was observed in a high percentage of patients, to variable extents, suggesting that the microenvironment of human PDAC is in fact permissive to the infiltration of lymphocytes and that strategies either enhancing their formation or activation status should be encouraged. From a clinical perspective, we could envisage the assessment of TLT as a potential approach to better allocate patients to immunotherapy.⁴⁸ Our study brings to light the critical duality displayed by immune cells according to their spatial organization in the tumor microenvironment, providing a different perspective compared to studies addressing the prognostic role of immune cells obtained by gene expression, FACS-based or tissue microarray analyses. Our findings underline the need of an integrated and comprehensive analysis of the immune microenvironment, performed by an objective and compartment-specific evaluation of immune populations.

The identification of histologically distinct immune components, i.e., PD1-GC and CD20-TLT, which concur in classifying PDAC patients according to the clinical outcome, is expected to have important implications in the design of clinical trials aimed at testing novel immunotherapeutic approaches. However, in human PDAC, immunotherapy is a promising alternative option to the poorly effective available treatments, but still far from being successfully adopted in the clinic, thus efforts remain focused on identifying patients who will receive clinical benefit from chemotherapy. A growing body of evidence suggests the interaction of immune cells with conventional anticancer therapies, including chemotherapy and radiation.^{49,50} Whether the presence of TLT could be instrumental to the efficacy of chemotherapy in human PDAC

still needs to be addressed but represents a relevant clinical question.

Materials and methods

Patients and study design

The study included 104 patients aged older than 18 years, diagnosed with PDAC and who consecutively underwent surgery at the Humanitas Clinical and Research Center, from February 2010 to December 2012. Clinicians prospectively assembled a clinical retrospective database by collecting patient demographics, clinical, and histopathological data, as detailed in Table S1. Investigators who performed the assessment of immune variables were blinded to the clinical data. Patients with metastases at surgery ($n = 7$) were excluded from the analysis. Detection of postsurgical local and distant tumor recurrences included a baseline thoracic and abdominal computed tomography (CT) and CA19-9 serum level evaluation. CT was repeated every 3 mo during the first two years after surgery, and every 6 mo afterward. CA19.9 assessment was repeated on a monthly basis during chemotherapy and concomitantly to CT scan afterward. As outcome variable we considered disease-specific survival (DSS), defined as any PDAC-related death detected in the observational period started immediately after surgery. Patients who died from causes other than PDAC were considered as lost to follow-up. The time of DSS was calculated from the date of surgery until date of death. The mean follow-up was 563.4 d (Standard Deviation = 320.8 d).

Immunohistochemistry

Human FFPE-PDAC tissues were provided as tissue blocks, by the Pathology Department of the Humanitas Clinical and Research Center. 2 μ m thick consecutive tissue sections were obtained from each specimen and stained as previously described.¹² In brief, sections were autostained (IntelliPATH FLX; Biocare Medical) with primary antibodies raised against CD20 (DAKO, L26), CD8 (DAKO, C8/144B), PD-1 (Abcam NAT105), CD3 (DAKO, F7.2.38), DC-Lamp (Dendritics, 1010E1.01), PNA β (BD PharMingen, MECA-79), Lyve-1 (Abcam, polyclonal), CXCL13 (R&D, polyclonal), CCL21 (R&D, polyclonal), IL-10 (R&D Systems, polyclonal), Ki67 (DAKO, MIB-1), Bcl-6 (DAKO, PG-B6p). Immunohistochemistry was performed with the same protocol on FFPE tissues from mouse pancreata. Primary antibodies used were: B220 (eBioscience, RA3-6B2), PD-1 (Novus Biologicals, polyclonal), CD3 (eBioscience, 145-2C11).

Image analysis

After staining procedure, tissue sections were digitalized using dotSlide (Olympus dotSlide). At least two independent operators blinded to any patient clinical data selected three non-overlapping and non-contiguous areas comprising of approximately 50% of tumor and 50% of stromal tissue and including CD20-TILs and CD8-TILs. For CD20-TLT analysis, three non-contiguous fields were chosen representing the entire CD20

positive area within the TLT, regardless of the location in the tumor or in the stroma. Both sampled microscopic area and light density were maintained fixed throughout the analysis. Selected areas were quantified by computer-assisted image analysis, with ad hoc software, to obtain the percentage of immune reactive areas (IRA%) of the digitalized tissue surface. The mean value, obtained from the three different regions was calculated for each immune variable and subsequently used for statistical purposes. The variable PD1-GC was expressed as a dichotomous value, assigning a positive value when PD1 positive cells were present in the GC of previously assessed CD20-TLT. The extent of the overall distribution of CD20-TLT, CD20-TIL, CD8-TIL IRA%, expressed as continuous variables, and PD1-GC score were used to perform statistical analyses. For each immune variable with continuous values (CD20-TLT, CD20-TILs, CD8-TILs), we stratified patients by grouping into quartiles.

Statistical analysis

The associations between values of CD20-TLT, CD20-TILs, CD8-TILs, PD-1-GC and other features concerning patient clinical conditions were estimated by Pearson simple linear regression analysis. A multivariate Cox proportional hazards model was developed to assess the role of immune variable density and demographic, clinical, and histopathologic features, in predicting the outcome of disease specific survival. Cox multivariate analysis was performed by entering variables with a *p* value less than 0.05 at univariate analysis. Kaplan–Meier curves of DSS were plotted and the log-rank test was used to compare the curves of each subgroup of patients with pancreatic cancer. For each test, only two-sided *P* values lower than 0.05 were considered statistically significant. All the analyses were done using SPSS (Version 22.0) and GraphPad Prism software (Version 4.1). To study the prognostic value of immune variables, we adhered to “Reporting Recommendations for Tumor Marker Prognostic Studies (REMARK)”⁵¹ for high quality of tumor marker studies.

Gene expression analysis

Patients were divided into TLT^{hi} (4th quartile) and TILs^{hi} (4th quartile), according to CD20-TLT and CD20-TIL IRA% values and RNA extracted from FFPE tissues using the RNeasy FFPE kit (QIAGEN). RNA from Panc02 tumors was extracted after collagenase (Sigma Aldrich) digestion of tumor fragments and isolation of the leukocyte fraction by gradient centrifugation (Percoll (GE Healthcare life sciences)). Cells were resuspended with PureZOL (Bio-Rad), and RNA was purified using RNeasy Plus Mini kit (QIAGEN) following manufacturer instructions. In both cases, cDNA was obtained after an eight cycles pre-amplification step, followed by reverse transcription with the RT² PreAMP cDNA synthesis kit (Qiagen). Real-Time PCR was performed using commercially available PCR Arrays (RT² Profiler™ PCR Array System, Qiagen), on a ViiA™ 7 Real-Time PCR (Life Technologies). Differences in gene expression were analyzed by the comparative threshold cycle (Ct) method with DataAssist™ (Life Technologies), after global normalization. Five samples of PDAC tumors from TLT^{hi} (4th quartile)

patients and four samples of PDAC tumors from TILs^{hi} (4th quartile) patients were analyzed. Within a specific group, samples with the lowest Ct variability (*n* = 3) were selected for analysis (Fig. S6). Adjacent normal pancreatic tissue (*n* = 3) was used as a control. Hierarchical clustering was performed with the Cluster 3.0 software,⁵² including the whole gene-list available in the Array. The normalized signal value was adjusted to log transform data and “median” was selected to center genes. Clustering was performed using the Pearson correlation function with Java TreeView⁵² and exported to heat-map images.

For the network analysis, uploading control and α -CD20-treated data set, containing gene identifiers and corresponding expression values, into the Ingenuity Pathways Analysis application generated significant pathways and molecular networks. The resulting Network Eligible molecules were overlaid onto a global molecular network based on the in Ingenuity’s Knowledge Base (Ingenuity® Systems, www.ingenuity.com), a uniquely structured repository of biological and chemical “findings” curated from various sources including the literature. The Functional Analysis of the network identified the biological functions most significant to the molecules in the network including the whole gene-list available in the Array.

PDAC murine models

All mice used for the orthotopic implantation of Panc02 cells were 8-week-old C57BL/6J females purchased from Charles River (Calco, Italy) and housed in a specific pathogen-free animal facility of the Humanitas Clinical and Research Center, in individually ventilated cages. Procedures involving mice and their care were conformed to EU and Institutional Guidelines. Murine Panc02 cell line was kindly provided by Dr. Piemonti (San Raffaele Hospital, Milan) and cultured in RPMI 1640 medium (Lonza) supplemented with 10% FBS, 2 mM L-Glutamine. Cells were cultured in a humidified incubator with 5% CO₂, for one passage before *in vivo* injection. Mice were kept anesthetized during all surgical operation by intraperitoneal administration of a ketamine and xylazine solution. The stomach and the adherent pancreas were exteriorized to expose the head of the pancreas, in which 30 μ L of 10⁶ Panc02 cell suspension was injected using a 30 gauge insulin needle. All the organs were then returned to their original position and peritoneum and skin sutured. Animals were randomized after surgery into two treatment groups, the first receiving 250 μ g of α -CD20 antibody (Genentech, clone 5D2), the second receiving 250 μ g of the isotype-matched (IgG2a) irrelevant immunoglobulin (BioXCell C1.18.4), both with i.p. injection 3 days after surgery. After 3 weeks from surgery, mice were sacrificed and tumor masses collected. Single-cell suspensions were obtained by incubating fragmented tumors with 0.5 mg/mL of clostridium histolyticum derived collagenase (Sigma Aldrich) for 30 min at 37°C. Cells were then washed and tumor-infiltrating leukocytes purified by a 44%/66% Percoll (GE Healthcare life sciences) gradient centrifugation. The purified leukocytes were washed and aliquoted for multicolor FACS analysis or RNA extraction. Alternatively, tissues were fixed for immunohistochemical analysis.

Pancreatic cancer-prone LSL-Kras^{G12D}-Pdx1-Cre mice (KC mice) were bred, maintained and treated at the saprophytic and pathogen-free animal facility of the Molecular Biotechnologies Center (Torino, Italy), as previously described.³⁶ Briefly, KC mice were vaccinated at 32 weeks of age and every 3 weeks for a total of three rounds of vaccination. Vaccination was achieved by electroporation with 50 μ g of plasmid (either mock pVAX vector or the human Enolase (ENO1) encoding vector), as previously described.³⁶ Mice of the same age were randomly assigned to control and treatment groups, and all groups were specifically treated concurrently. Mice were sacrificed 2 weeks after the last vaccination to perform histologic or immunohistochemical analyses. Splenocytes were analyzed for the ability to secrete IFN γ in response to the recombinant ENO1 *ex vivo*.³⁶

Flow cytometry

Absolute numbers of CD19⁺, CD3⁺, CD11b⁺ cells were assessed by flow cytometry on peripheral blood leukocytes at day 0, 3, 7, 14 and 21 d from antibody injection. Trucount kit (BD Biosciences) was used to obtain absolute numbers. The following fluorophore-conjugated primary antibodies were used: anti-CD45 (BD PharMingen 30-F11), anti-CD19 (eBiosciences eBio1D3), anti-CD3 (eBiosciences 145-2C11), anti-CD11b (BioLegend M1/70). Sample acquisition was performed on a BD LSRFORTESSA (BD Biosciences) and data analyzed with FlowJo software.

Disclosure of potential conflicts of interest

No potential conflicts of interest were disclosed.

Acknowledgments

We are grateful to Professor Alberto Mantovani for critical suggestions and review of the manuscript.

Funding

This work was supported by the Humanitas Clinical and Research Center (grant Translation in Medical Oncology 2013 to FM and AZ), the Italian Ministry of University and Research, (FIRB grant RBAP11H2R9), Associazione Italiana Ricerca sul Cancro (AIRC 5 \times 1000 IG-12182 to PA and FN and IG 15257 to FN), Fondazione Italiana Ricerca sul Cancro (iCare fellowship to GDC). The funders had no role in study design, data collection and analysis, decision to publish, or preparation of the manuscript.

References

- Siegel R, Ma J, Zou Z, Jemal A. Cancer statistics, 2014. *CA Cancer J Clin* 2014; 64:9-29; PMID:24399786; <http://dx.doi.org/10.3322/caac.21208>
- Conroy T, Desseigne F, Ychou M, Bouche O, Guimbaud R, Becouarn Y, Adenis A, Raoul JL, Gourgou-Bourgade S, de la Fouchardiere C et al. FOLFIRINOX versus gemcitabine for metastatic pancreatic cancer. *N Engl J Med* 2011; 364:1817-25; PMID:21561347; <http://dx.doi.org/10.1056/NEJMoa1011923>
- Clark CE, Hingorani SR, Mick R, Combs C, Tuveson DA, Vonderheide RH. Dynamics of the immune reaction to pancreatic cancer from inception to invasion. *Cancer Res* 2007; 67:9518-27; PMID:17909062; <http://dx.doi.org/10.1158/0008-5472.CAN-07-0175>
- Vonderheide RH, Bayne LJ. Inflammatory networks and immune surveillance of pancreatic carcinoma. *Curr Opin Immunol* 2013; 25:200-5; PMID:23422836; <http://dx.doi.org/10.1016/j.coi.2013.01.006>
- Ene-Obong A, Clear AJ, Watt J, Wang J, Fatah R, Riches JC, Marshall JF, Chin-Aleong J, Chelala C, Gribben JG et al. Activated pancreatic stellate cells sequester CD8 +T cells to reduce their infiltration of the juxtatumoral compartment of pancreatic ductal adenocarcinoma. *Gastroenterology* 2013; 145:1121-32; PMID:23891972; <http://dx.doi.org/10.1053/j.gastro.2013.07.025>
- Beatty GL, Chiorean EG, Fishman MP, Saboury B, Teitelbaum UR, Sun W, Huhn RD, Song W, Li D, Sharp LL et al. CD40 agonists alter tumor stroma and show efficacy against pancreatic carcinoma in mice and humans. *Science* 2011; 331:1612-6; PMID:21436454; <http://dx.doi.org/10.1126/science.1198443>
- Laheru D, Jaffee EM. Immunotherapy for pancreatic cancer - science driving clinical progress. *Nat Rev Cancer* 2005; 5:459-67; PMID:15905855; <http://dx.doi.org/10.1038/nrc1630>
- Ozdemir BC, Pentcheva-Hoang T, Carstens JL, Zheng X, Wu CC, Simpson TR, Laklai H, Sugimoto H, Kahlert C, Novitskiy SV et al. Depletion of carcinoma-associated fibroblasts and fibrosis induces immunosuppression and accelerates pancreas cancer with reduced survival. *Cancer Cell* 2014; 25:719-34; PMID:24856586; <http://dx.doi.org/10.1016/j.ccr.2014.04.005>
- Ogino S, Galon J, Fuchs CS, Dranoff G. Cancer immunology-analysis of host and tumor factors for personalized medicine. *Nat Rev Clin Oncol* 2011; 8:711-9; PMID:21826083; <http://dx.doi.org/10.1038/nrcli.nonc.2011.122>
- Galon J, Angell HK, Bedognetti D, Marincola FM. The continuum of cancer immunosurveillance: prognostic, predictive, and mechanistic signatures. *Immunity* 2013; 39:11-26; PMID:23890060; <http://dx.doi.org/10.1016/j.immuni.2013.07.008>
- Galon J, Costes A, Sanchez-Cabo F, Kirilovsky A, Mlecnik B, Lagorce-Pages C, Tosolini M, Camus M, Berger A, Wind P et al. Type, density, and location of immune cells within human colorectal tumors predict clinical outcome. *Science* 2006; 313:1960-4; PMID:17008531; <http://dx.doi.org/10.1126/science.1129139>
- Di Caro G, Bergomas F, Grizzi F, Doni A, Bianchi P, Malesci A, Laghi L, Allavena P, Mantovani A, Marchesi F. Occurrence of tertiary lymphoid tissue is associated with T-cell infiltration and predicts better prognosis in early-stage colorectal cancers. *Clin Cancer Res* 2014; 20:2147-58; PMID:24523438; <http://dx.doi.org/10.1158/1078-0432.CCR-13-2590>
- Fridman WH, Pages F, Sautes-Fridman C, Galon J. The immune contexture in human tumours: impact on clinical outcome. *Nat Rev Cancer* 2012; 12:298-306; PMID:22419253; <http://dx.doi.org/10.1038/nrc3245>
- Ogino S, Noshio K, Irahara N, Meyerhardt JA, Baba Y, Shima K, Glickman JN, Ferrone CR, Mino-Kenudson M, Tanaka N et al. Lymphocytic reaction to colorectal cancer is associated with longer survival, independent of lymph node count, microsatellite instability, and CpG island methylator phenotype. *Clin Cancer Res* 2009; 15:6412-20; PMID:19825961; <http://dx.doi.org/10.1158/1078-0432.CCR-09-1438>
- Dieu-Nosjean MC, Antoine M, Danel C, Heudes D, Wislez M, Poulot V, Rabbe N, Laurans L, Tartour E, de Chaisemartin L et al. Long-term survival for patients with non-small-cell lung cancer with intratumoral lymphoid structures. *J Clin Oncol* 2008; 26:4410-7; PMID:18802153; <http://dx.doi.org/10.1200/JCO.2007.15.0284>
- Coppola D, Nebozhyn M, Khalil F, Dai H, Yeatman T, Loboda A, Mule JJ. Unique ectopic lymph node-like structures present in human primary colorectal carcinoma are identified by immune gene array profiling. *Am J Pathol* 2011; 179:37-45; PMID:21703392; <http://dx.doi.org/10.1016/j.ajpath.2011.03.007>
- Cipponi A, Mercier M, Seremet T, Baurain JF, Theate I, van den Oord J, Stas M, Boon T, Coulie PG, van Baren N. Neogenesis of lymphoid structures and antibody responses occur in human melanoma metastases. *Cancer Res* 2012; 72:3997-4007; PMID:22850419; <http://dx.doi.org/10.1158/0008-5472.CAN-12-1377>

18. Di Caro G, Castino GF, Bergomas F, Cortese N, Chiriva-Internati M, Grizzi F, Mantovani A, Marchesi F. Tertiary lymphoid tissue in the tumor microenvironment: from its occurrence to immunotherapeutic implications. *Int Rev Immunol* 2015; 34:123–33; PMID:25901857; <http://dx.doi.org/10.3109/08830185.2015.1018416>
19. de Chaisemartin L, Goc J, Damotte D, Validire P, Magdeleinat P, Alifano M, Cremer I, Fridman WH, Sautes-Fridman C, Dieu-Nosjean MC. Characterization of chemokines and adhesion molecules associated with T cell presence in tertiary lymphoid structures in human lung cancer. *Cancer Res* 2011; 71:6391–9; PMID:21900403; <http://dx.doi.org/10.1158/0008-5472.CAN-11-0952>
20. Germain C, Gnjatich S, Tamzalit F, Knockaert S, Remark R, Goc J, Lepelletier A, Becht E, Katsahian S, Bizouard G et al. Presence of B Cells in Tertiary Lymphoid Structures is Associated with a Protective Immunity in Lung Cancer Patients. *Am J Respir Crit Care Med* 2014; 189(7):832–44; PMID:24484236; <http://dx.doi.org/10.1164/rccm.201309-1611OC>
21. Dieu-Nosjean MC, Goc J, Giraldo NA, Sautes-Fridman C, Fridman WH. Tertiary lymphoid structures in cancer and beyond. *Trends Immunol* 2014; 35(11):571–80; PMID:25443495; <http://dx.doi.org/10.1016/j.it.2014.09.006>
22. Goc J, Germain C, Vo-Bourgeois TK, Lupo A, Klein C, Knockaert S, de Chaisemartin L, Ouakrim H, Becht E, Alifano M et al. Dendritic cells in tumor-associated tertiary lymphoid structures signal a Th1 cytotoxic immune contexture and license the positive prognostic value of infiltrating CD8+ T cells. *Cancer Res* 2014; 74:705–15; PMID:24366885; <http://dx.doi.org/10.1158/0008-5472.CAN-13-1342>
23. de Visser KE, Korets LV, Coussens LM. De novo carcinogenesis promoted by chronic inflammation is B lymphocyte dependent. *Cancer Cell* 2005; 7:411–23; PMID:15894262; <http://dx.doi.org/10.1016/j.ccr.2005.04.014>
24. Nelson BH. CD20+ B cells: the other tumor-infiltrating lymphocytes. *J Immunol* 2010; 185:4977–82; PMID:20962266; <http://dx.doi.org/10.4049/jimmunol.1001323>
25. Bindea G, Mlecnik B, Tosolini M, Kirilovsky A, Waldner M, Obenauf AC, Angell H, Fredriksen T, Lafontaine L, Berger A et al. Spatiotemporal dynamics of intratumoral immune cells reveal the immune landscape in human cancer. *Immunity* 2013; 39:782–95; PMID:24138885; <http://dx.doi.org/10.1016/j.immuni.2013.10.003>
26. Affara NI, Ruffell B, Medler TR, Gunderson AJ, Johansson M, Bornstein S, Bergsland E, Steinhoff M, Li Y, Gong Q et al. B cells regulate macrophage phenotype and response to chemotherapy in squamous carcinomas. *Cancer Cell* 2014; 25:809–21; PMID:24909985; <http://dx.doi.org/10.1016/j.ccr.2014.04.026>
27. Lund FE, Randall TD. Effector and regulatory B cells: modulators of CD4+ T cell immunity. *Nat Rev Immunol* 2010; 10:236–47; PMID:20224569; <http://dx.doi.org/10.1038/nri2729>
28. Fremd C, Schuetz F, Sohn C, Beckhove P, Domschke C. B cell-regulated immune responses in tumor models and cancer patients. *Oncoimmunology* 2013; 2(7):e25443; PMID:24073382; <http://dx.doi.org/10.4161/onci.25443>
29. Hannani D, Locher C, Yamazaki T, Colin-Minard V, Vetizou M, Aymeric L, Viaud S, Sanchez D, Smyth MJ, Bruhns P et al. Contribution of humoral immune responses to the antitumor effects mediated by anthracyclines. *Cell Death Differ* 2014; 21:50–8; PMID:23744294; <http://dx.doi.org/10.1038/cdd.2013.60>
30. Shalapour S, Font-Burgada J, Di Caro G, Zhong Z, Sanchez-Lopez E, Dhar D, Willimsky G, Ammirante M, Strasner A, Hansel DE et al. Immunosuppressive plasma cells impede T-cell-dependent immunogenic chemotherapy. *Nature* 2015; 521:94–8; PMID:25924065; <http://dx.doi.org/10.1038/nature14395>
31. Carmi Y, Spitzer MH, Linde IL, Burt BM, Prestwood TR, Perlman N, Davidson MG, Kenkel JA, Segal E, Pusapati GV et al. Allogeneic IgG combined with dendritic cell stimuli induce antitumor T-cell immunity. *Nature* 2015; 521:99–104; PMID:25924063; <http://dx.doi.org/10.1038/nature14424>
32. Schaerli P, Willmann K, Lang AB, Lipp M, Loetscher P, Moser B. CXC chemokine receptor 5 expression defines follicular homing T cells with B cell helper function. *J Exp Med* 2000; 192:1553–62; PMID:11104798; <http://dx.doi.org/10.1084/jem.192.11.1553>
33. Breitfeld D, Ohl L, Kremmer E, Ellwart J, Sallusto F, Lipp M, Forster R. Follicular B helper T cells express CXC chemokine receptor 5, localize to B cell follicles, and support immunoglobulin production. *J Exp Med* 2000; 192:1545–52; PMID:11104797; <http://dx.doi.org/10.1084/jem.192.11.1545>
34. Good-Jacobson KL, Szumilas CG, Chen L, Sharpe AH, Tomayko MM, Shlomchik MJ. PD-1 regulates germinal center B cell survival and the formation and affinity of long-lived plasma cells. *Nat Immunol* 2010; 11:535–42; PMID:20453843; <http://dx.doi.org/10.1038/ni.1877>
35. Gu-Trantien C, Loi S, Garaud S, Equeter C, Libin M, de Wind A, Ravoet M, Le Buanec H, Sibille C, Manfouo-Foutsop G et al. CD4 (+) follicular helper T cell infiltration predicts breast cancer survival. *J Clin Invest* 2013; 123:2873–92; PMID:23778140; <http://dx.doi.org/10.1172/JCI67428>
36. Cappello P, Rolla S, Chiarle R, Principe M, Cavallo F, Perconti G, Feo S, Giovarelli M, Novelli F. Vaccination with ENO1 DNA prolongs survival of genetically engineered mice with pancreatic cancer. *Gastroenterology* 2013; 144:1098–106; PMID:23333712; <http://dx.doi.org/10.1053/j.gastro.2013.01.020>
37. Gunderson AJ, Coussens LM. B cells and their mediators as targets for therapy in solid tumors. *Exp Cell Res* 2013; 319(11):1644–9; PMID:23499742; <http://dx.doi.org/10.1016/j.yexcr.2013.03.005>
38. Vesely MD, Kershaw MH, Schreiber RD, Smyth MJ. Natural innate and adaptive immunity to cancer. *Annu Rev Immunol* 2011; 29:235–71; PMID:21219185; <http://dx.doi.org/10.1146/annurev-immunol-031210-101324>
39. Barbera-Guillem E, Nelson MB, Barr B, Nyhus JK, May KFJ, Feng L, Sampsel JW. B lymphocyte pathology in human colorectal cancer. Experimental and clinical therapeutic effects of partial B cell depletion. *Cancer Immunol Immunother* 2000; 48:541–9; PMID:10630306; <http://dx.doi.org/10.1007/PL00006672>
40. Aklilu M, Stadler WM, Markiewicz M, Vogelzang NJ, Mahowald M, Johnson M, Gajewski TF. Depletion of normal B cells with rituximab as an adjunct to IL-2 therapy for renal cell carcinoma and melanoma. *Ann Oncol* 2004; 15:1109–14; PMID:15205206; <http://dx.doi.org/10.1093/annonc/mdh280>
41. Martin F, Chan AC. B cell immunobiology in disease: evolving concepts from the clinic. *Annu Rev Immunol* 2006; 24:467–96; PMID:16551256; <http://dx.doi.org/10.1146/annurev.immunol.24.021605.090517>
42. Thauanot A, Patey N, Gautreau C, Lechaton S, Fremaux-Bacchi V, Dieu-Nosjean MC, Cassuto-Viguier E, Legendre C, Delahousse M, Lang P et al. B cell survival in intra-graft tertiary lymphoid organs after rituximab therapy. *Transplantation* 2008; 85:1648–53; PMID:18551073; <http://dx.doi.org/10.1097/TP.0b013e3181735723>
43. Schietinger A, Greenberg PD. Tolerance and exhaustion: defining mechanisms of T cell dysfunction. *Trends Immunol* 2014; 35(2):51–60; PMID:24210163; <http://dx.doi.org/10.1016/j.it.2013.10.001>
44. Topalian SL, Drake CG, Pardoll DM. Targeting the PD-1/B7-H1 (PD-L1) pathway to activate anti-tumor immunity. *Curr Opin Immunol* 2012; 24:207–12; PMID:22236695; <http://dx.doi.org/10.1016/j.coi.2011.12.009>
45. Gros A, Robbins PF, Yao X, Li YF, Turcotte S, Tran E, Wunderlich JR, Mixon A, Farid S, Dudley ME et al. PD-1 identifies the patient-specific CD8(+) tumor-reactive repertoire infiltrating human tumors. *J Clin Invest* 2014; 124:2246–59; PMID:24667641; <http://dx.doi.org/10.1172/JCI73639>
46. Gajewski TF, Schreiber H, Fu YX. Innate and adaptive immune cells in the tumor microenvironment. *Nat Immunol* 2013; 14:1014–22; PMID:24048123; <http://dx.doi.org/10.1038/ni.2703>
47. Lutz ER, Wu AA, Bigelow E, Sharma R, Mo G, Soares K, Solt S, Dorman A, Wamwea A, Yager A et al. Immunotherapy converts nonimmunogenic pancreatic tumors into immunogenic foci of immune regulation. *Cancer Immunol Res* 2014; 2:616–31; PMID:24942756; <http://dx.doi.org/10.1158/2326-6066.CIR.14-0027>
48. Messina JL, Fenstermacher DA, Eschrich S, Qu X, Berglund AE, Lloyd MC, Schell MJ, Sondak VK, Weber JS, Mule JJ. Twelve-Chemokine gene signature identifies lymph node-like structures in melanoma: potential for patient selection for immunotherapy? *Sci Rep* 2012; 2:765; PMID:23097687; <http://dx.doi.org/10.1038/srep00765>

49. Galluzzi L, Vacchelli E, Bravo-San Pedro JM, Buque A, Senovilla L, Baracco EE, Bloy N, Castoldi F, Abastado JP, Agostinis P et al. Classification of current anticancer immunotherapies. *Oncotarget* 2014; 5:12472–508; PMID:25537519; <http://dx.doi.org/10.18632/oncotarget.2998>
50. Mantovani A, Allavena P. The interaction of anticancer therapies with tumor-associated macrophages. *J Exp Med* 2015; 212(4):435–45; PMID:25753580; <http://dx.doi.org/10.1084/jem.20150295>
51. Altman DG, McShane LM, Sauerbrei W, Taube SE. Reporting Recommendations for Tumor Marker Prognostic Studies (REMARK): explanation and elaboration. *PLoS Med* 2012; 9:e1001216; PMID:22675273; <http://dx.doi.org/10.1371/journal.pmed.1001216>
52. Eisen MB, Spellman PT, Brown PO, Botstein D. Cluster analysis and display of genome-wide expression patterns. *Proc Natl Acad Sci U S A* 1998; 95:14863–8; PMID:9843981; <http://dx.doi.org/10.1073/pnas.95.25.14863>